Holistic Evaluation of Involute Gears

Anita Przyklenk, Tom Reavie, Martin Stein and Robert Frazer

State of the Art in Gear Metrology

Gear evaluation strategies for testing the surface geometry of involute gears are commonly carried out according to the standard ISO 1328-1 (Ref. 1) and VDI/VDE guidelines aiming for the determination of helix, profile (Ref. 2) and pitch deviations (Ref. 3). These deviations refer to single helix, profile line, and pointwise inspections of specific gear teeth, which is sufficient in most cases and has been demonstrated by international intercomparisons (Refs. 4, 5). The deviations on the gear flanks are caused by manufacturing defects due to various error sources. Therefore, identifying these error sources is essential for the improvement of manufacturing processes.

Two different types of defects can occur during the manufacturing process (Refs. 6, 7). First, systematic defects caused by the positioning of the tool, tool wear, or other sources. This results in the same, reoccurring deviation on each tooth. Therefore, the associated systematic manufacturing defect can be specified, if only single teeth are tested. Second, individual defects caused by changing conditions during the manufacturing process like temperature gradients, tool vibrations, spindle positioning errors and other drifting effects. Individual manufacturing defects can occur on any tooth and can only be accurately evaluated if all teeth are tested (e.g. Ref. 7). In order to characterize different sources of defects properly, measurements should refer to a common reference coordinate system, and an error separation method has to be applied. However, error separation is most efficiently achieved when all measurements have taken place in the same reference coordinate system. A common reference system would also lead to a more accurate determination of the deviations. So far, this approach has not been established in gear metrology.

As well as evaluation of profile, helix and pitch deviations, harmonic analysis of measured 2D trace data is routinely used by some industries to control gear noise (Refs. 8–10) and characterize machine tool performance (Refs. 11, 12). Evaluation of 3D surface measurement data has not been investigated.

Introduction

This article consists of two parts: holistic evaluation and residual analysis. The first part is on the holistic gear surface evaluation approach, where the 3D model strategy is introduced, followed by a description of the holistic evaluation algorithm and one application example. By means of the application example, two possibilities are presented which use different determined geometry parameters to describe the gear surface. In the second part (Analysis of Harmonic Content), obtained residuals of both inversion methods are analyzed regarding their harmonic content by means of discrete fast Fourier transformation (FFT) and discrete wavelet transformation (DWT). These transformations are introduced in the simpler 2D case using synthetic and measured data, then expanded to 3D using pseudo-measured data. Figure 1 gives an overview on the structure of this article.

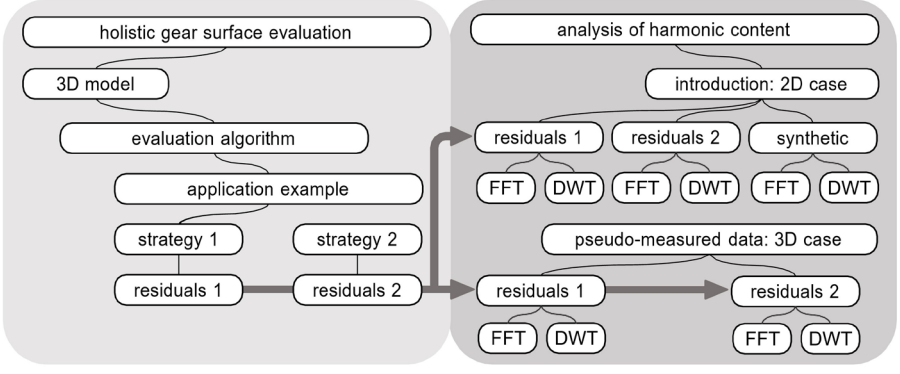

Figure 1 Structure of the presented work.

Holistic Gear Surface Evaluation

3D-Gear Model Strategy

A three-dimensional surface model according to Härtig and Stein in their article "3D involute gear evaluation — Part I: Workpiece coordinates," (Ref. 13) has been applied as a so-called form element, which is an essential part of the inversion algorithm's objective function. The origin of the coordinate system is located on the center of the non-datum face. The Cartesian coordinates (x,y,z) on the gear surface are described by involute coordinates (r, φ_b, z). Therefore, the involute gear's surface is expressed with

$$\begin{aligned} x &= r \cdot \cos(\varphi_b + hand \cdot c \cdot z + flank \cdot \mathrm{inv}(\alpha_t)) \\ y &= r \cdot \sin(\varphi_b + hand \cdot c \cdot z + flank \cdot \mathrm{inv}(\alpha_t)) \\ z &= z \end{aligned} \tag{1}$$

where *hand* and *flank* denote the slope direction and the tooth flank direction, respectively. The following relations apply:

- radius r in mm
  $$r = r_b / \cos(\alpha_t) \tag{2}$$
  with the base radius r_b in mm and the transverse pressure angle a*t* in rad
- helix coefficient in mm/mm describes the value of the helical slope

$$c = \tan(\beta_b)/r_b \quad (3)$$

with the helix angle at base circle βb in rad

- involute function in the transverse plane in rad

$$\mathrm{inv}(\alpha_t) = \tan(\alpha_t) - \alpha_t \quad (4)$$

with the transverse pressure angle αt in rad

The relation between the transverse pressure angle α_t and the radii is as follows

$$\alpha_t = \arccos(r_b/r) \quad (5)$$

Holistic Gear Evaluation Algorithm

In order to realize holistic gear evaluations, a three-dimensional object-orientated inversion algorithm has been implemented in *MATLAB*. The core of the algorithm is based on the approach by Sourlier and Bucher in their article "Exact best fit algorithm applicable to sculptured surfaces or to any non-regular surfaces in parametric form," (Ref. 14) aiming to fit parameterized form elements S into a measured point cloud $P_n = (x_n, y_n, z_n)$ that is composed of helix and profile measurements of all gear flanks, by solving a non-linear least squares problem with the Gauss-Newton method. A special feature of this approach is the distinction between three kinds of degrees of freedom. Those are the running parameters of the parameterized involute gear surface summarized in matrix $U = (z, \alpha_t)$, the geometry parameters represented in parameter vector $p = (r_b, \varphi_b, \beta_b)$ and the pose parameters to enable rotations and translations by applying a rotation matrix A and a translation matrix T on the form element during the inversion respectively.

This method allows the separation of dimension, form and pose. If, in addition, the helix and profile line measurements of gear surfaces were carried out in a common reference system, an error separation procedure is applied automatically. This allows an enhanced determination of deviations leading to an improved ability to determine manufacturing defects.

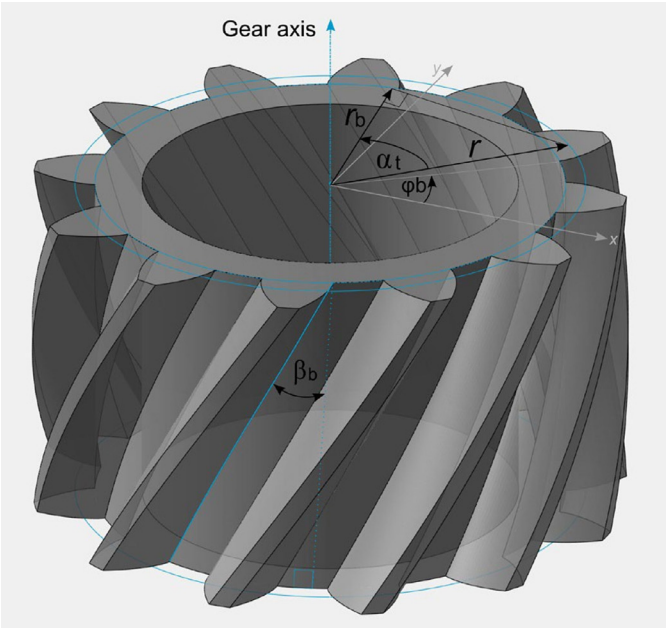

Figure 2 Involute gear with its coordinate system and geometry parameters.

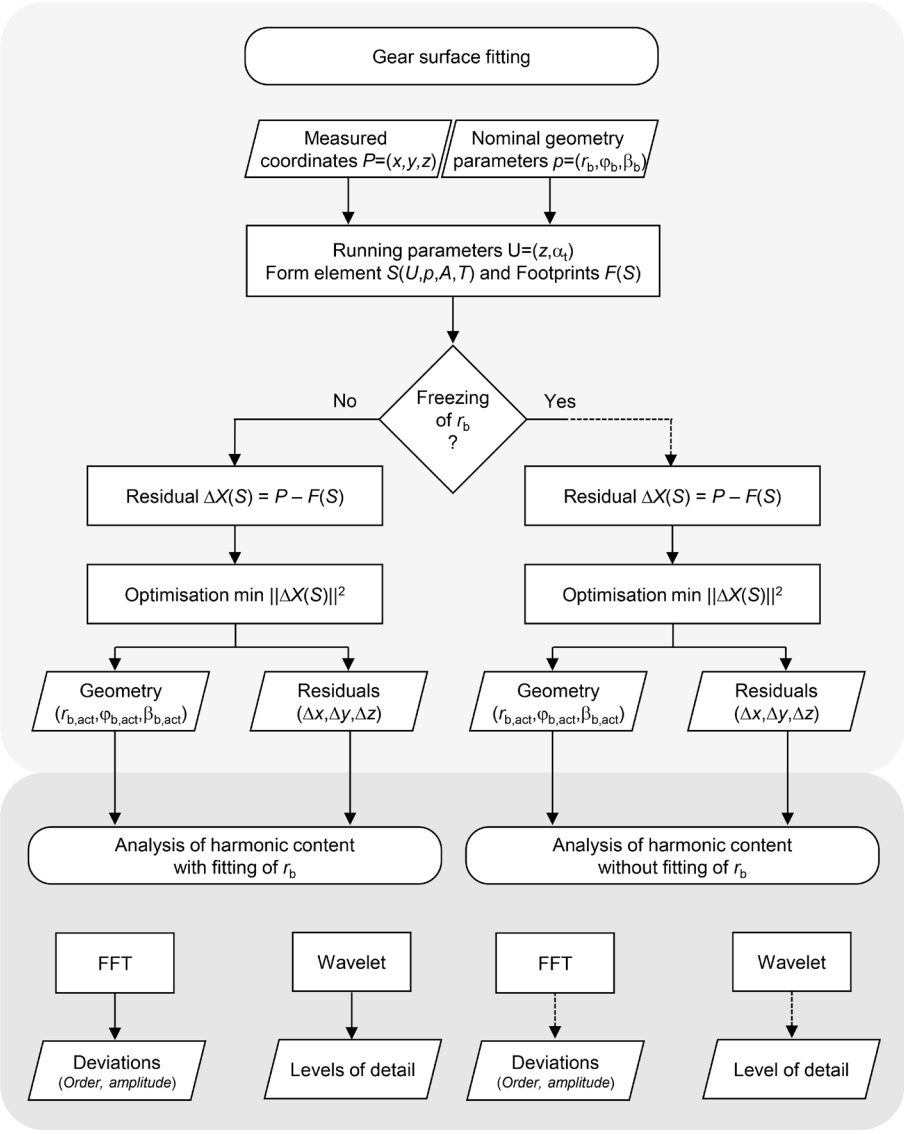

Figure 3 Flowchart of the holistic evaluation approach.

The objective function consists of residuals calculated by the difference between n measured points P_n and n projected foot points $F_n(S)$ on the surface of the shape element $S(U,p,A,T)$.

$$\Delta X_n(S) = P_n - F_n(S). \quad (6)$$

The objective function to be minimized is calculated with

$$\min \|\Delta X_n(S)\|2 \quad (7)$$

where ||...|| denotes that the Euclidian norm has been applied.

The optimization process is finished as soon as one of two defined termination criteria is achieved. Either when the specified maximum value for the iterations is reached, which is 25, or after the threshold for the solution update is reached, which is 10^{-12} mm.

The obtained inversion result consists of geometry parameter sets for each individual gear flank and the associated residuals.

In order to provide a connection to conventional evaluation procedures two possible settings have been implemented. Firstly, the algorithm also applies to 2D-single helix and 2D-profile measurement evaluations. Secondly, there is the possibility to freeze specific parameters during the inversion process. For example, the base radius can be set to be nominal and consequently would not be taken into account as with conventional evaluations.

In the second stage of the novel evaluation method, the determined geometry parameters and the corresponding residuals were used to perform an analysis of the harmonic content on the shape deviations. For this purpose, the 3D-residuals have been unwound over their reference lengths and analyzed by means of fast Fourier transformation (FFT) and discrete wavelet transform (DWT) as discussed in the second part of this paper. The final result is a set of deviations described by order and amplitude (FFT) and level of detail (DWT). Figure 3 shows the workflow of the evaluation steps by means of a flowchart.

Application Example

A workpiece-like artifact featuring different types of microgeometry corrections (also referred to as flank modifications) has been measured on a high-precision coordinate measuring machine under temperature-controlled laboratory conditions with $T = 20°C \pm 0.2K$. The nominal parameters of the artifact are summarized in Table 1 and Figure 4 shows a photo of the artifact.

Nine helix line and nine profile line measurements were carried out on each flank. A total of 432 lines were measured to map the surface of the 24

Table 1 Nominal gear parameters of the artifact

Number of teeth N	12
normal module mn/mm	12.000
normal pressure angle an/deg	20.0000
helix angle β/deg	30.0000
base circle diameter/mm	153.289
facewidth b/mm	110.000

Figure 4 Gear artifact.

Table 2 Overview of inversion results, which are the geometry parameters rb, jb and bb for 24 flanks of the twelve gear teeth. Nominal rb is put in brackets.

tooth	r_b fitted	r_b le/mm	φ_b le/rad	β_b le/rad	r_b ri/mm	φ_b ri/rad	β_b ri/rad
1	yes	76.650302	6.236183	0.489148	76.628715	5.856188	0.488996
	no	(76.644581)	6.236219	0.489117	(76.644581)	5.856287	0.489083
2	yes	76.636606	5.712631	0.489043	76.626965	5.332570	0.488983
	no	(76.644581)	5.712581	0.489085	(76.644581)	5.332680	0.489080
3	yes	76.637858	5.189084	0.489078	76.633454	4.809085	0.489018
	no	(76.644581)	5.189055	0.489114	(76.644581)	4.809155	0.489079
4	yes	76.631840	4.665440	0.489074	76.626543	4.285656	0.488958
	no	(76.644581)	4.665359	0.489142	(76.644581)	4.285769	0.489057
5	yes	76.635290	4.141934	0.489057	76.630183	3.761839	0.489033
	no	(76.644581)	4.141876	0.489107	(76.644581)	3.761929	0.489112
6	yes	76.631258	3.618153	0.489076	76.624655	3.238284	0.488978
	no	(76.644581)	3.618069	0.489147	(76.644581)	3.238409	0.489088
7	yes	76.632840	3.094693	0.489063	76.628654	2.714682	0.488999
	no	(76.644581)	3.094619	0.489125	(76.644581)	2.714782	0.489086
8	yes	76.642853	2.570870	0.489177	76.636152	2.191390	0.488972
	no	(76.644581)	2.570859	0.489187	(76.644581)	2.191443	0.489019
9	yes	76.634810	2.047368	0.489043	76.632809	1.667267	0.489020
	no	(76.644581)	2.047306	0.489095	(76.644581)	1.667341	0.489085
10	yes	76.639058	1.523792	0.489123	76.632667	1.143961	0.488982
	no	(76.644581)	1.523757	0.489153	(76.644581)	1.144036	0.489047
11	yes	76.655610	1.000059	0.489168	76.648719	0.620139	0.489112
	no	(76.644581)	1.000128	0.489109	(76.644581)	0.620113	0.489089
12	yes	76.655627	0.476441	0.489193	76.648067	0.096674	0.489117
	no	(76.644581)	0.476511	0.489134	(76.644581)	0.096652	0.489098

gear flanks. The density of the scanned points is specified by the difference of neighbored measuring points on the surface by means of the running parameters a*t* and *z*. The minimum helix and profile line angular resolution is ≈0.6 rad and along the *z*-coordinate ≈1.1 mm and ≈11 mm respectively.

The gathered lines are collected in one single point cloud and have been evaluated as described in the Holistic Gear Evaluation Algorithm section, above.

Geometry Parameters

In order to figure out individual manufacturing errors, fitted geometry parameters are available for each tooth per its left and right flank. The evaluation was carried out as illustrated in Figure 3. In one case r_b has been fitted ($r_{b,act}$) and in another case r_b was frozen at the nominal value ($r_{b,nom}$). A summary of the data of the determined geometry parameters is given in Table 2.

Nominal r_b is larger than the actual fitted with the exception of teeth 1, 11 and 12. The largest difference is on tooth 6 with $\Delta r_b = r_{b,act} - r_{b,nom} = 13.323\,\mu m$ at the left flank and $\Delta r_b = 19.926\,\mu m$ at the right flank. The smallest differences are located on the left flank of tooth 8 with $\Delta r_b = 5.523\,\mu m$ and on the right flank of tooth 12 with $\Delta r_b = 3.486\,\mu m$.

This difference is shown for all determined geometry parameters $\Delta = p_{act} - pnom$ in dependence of the tooth number in Figure 5. Figure 5a shows the difference of radii on left flanks. Those of φ_b and β_b are illustrated in Figure 3b. Figure 5c and 5d show corresponding results for the right flanks.

Whenever $r_{b,nom}$ does not meet $r_{b,act}$, the inversion algorithm tried to compensate this misfit by adapting the other geometry parameters φ_b and β_b. For instance, in Figure 5a Δr_b is positive on tooth 4, which means that $r_{b,nom}$ is larger than the actual $r_{b,act}$. This leads to a reduced φ_b in Figure 5b and to an enlarged φ_b in Figure 5d.

The effect is reversed when the nominal value is smaller than the actual one, as indicated by tooth 11 and 12 in Figure 5a and Figure 5c. The left flank has been fitted with an enlarged φ_b in Figure 5b and a reduced φ_b in Figure 5d.

If r_b is not fitted, then the influence on the angles is observed on all teeth with one exception that is tooth 1.

The correlation between $\Delta\beta_b$ and Δr_b is caused by the relationship given in Equation 2. To achieve a certain value for the actual helical slope, β_b has to be increased if nominal $r_{b,nom}$ is larger than $r_{b,act}$ and has to be decreased if $r_{b,nom}$ is smaller than $r_{b,act}$. This correlation is observed for left and right gear flanks.

Residuals and Form Deviations

In addition to the determined geometry parameters, the residuals $DX(S)$ of the holistic evaluation according to Equation 6 were also examined. Figure 6 depicts $DX(S)$ in µm obtained by inversion with fitting of r_b. $DX(S)$ is shown at the position of the form element S with color coding. Red denotes plus metal and blue minus metal. In the green areas $DX(S)$ approaches to zero. Individual manufacturing deviations on each tooth flank are represented in one single reference coordinate system. Some of the teeth (4,6,7,8,10,12) are obviously manufactured with helix crowning. On the basis of $DX(S)$ introduced here, the enhanced determination approach of profile deviations is described in the section "Analysis of Harmonic Content," below.

A comparison of the foot points on the shape element $F(S)$ acquired by

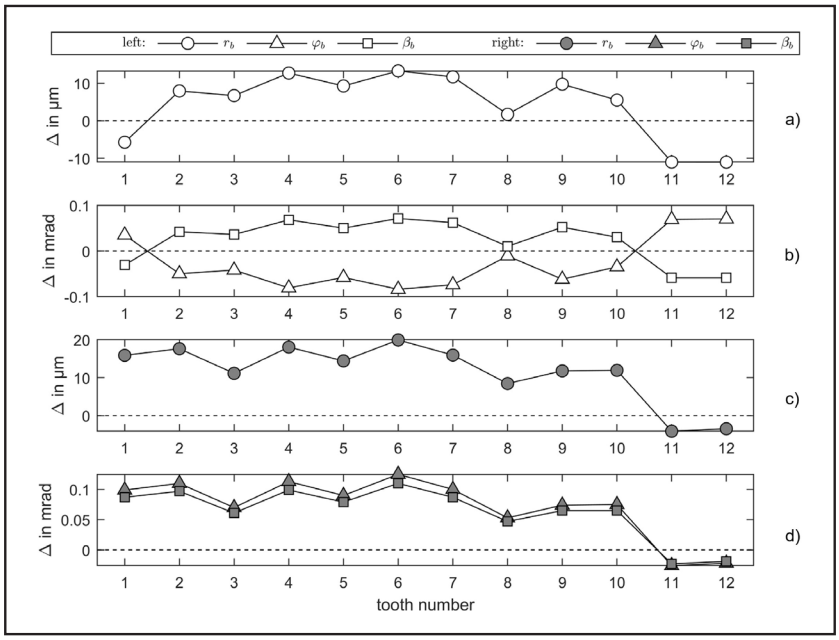

Figure 5 Differences between geometry parameters obtained with and without fitting rb.

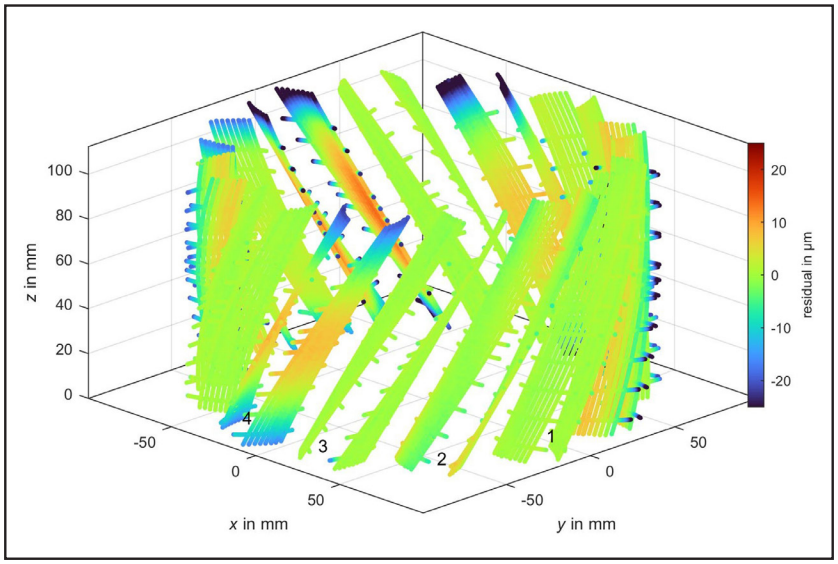

Figure 6 Residuals obtained by the inversion result with base radius fitting. Tooth 1 to 4 are labeled.

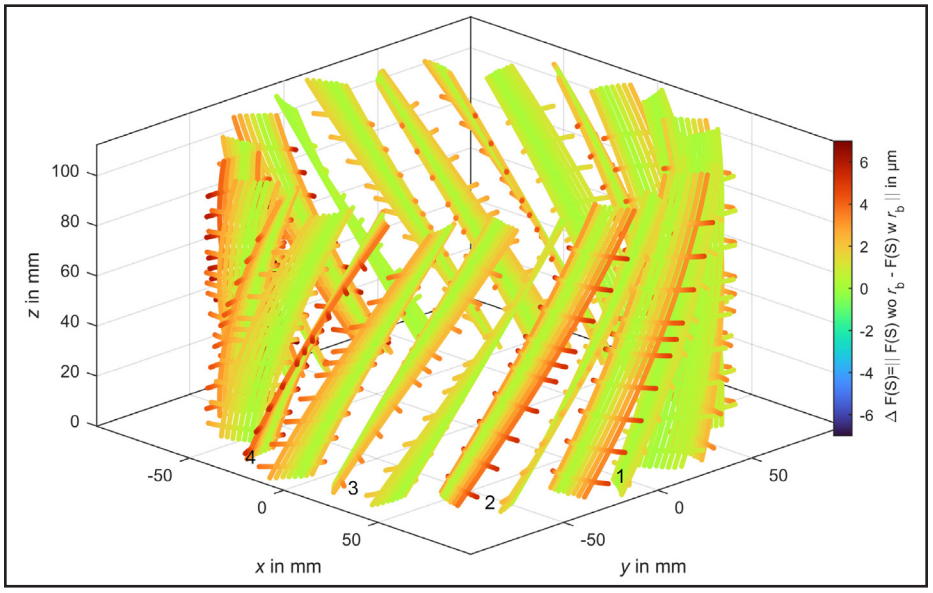

Figure 7 Difference between obtained foot points without and with fitting. Tooth 1 to 4 are labeled.

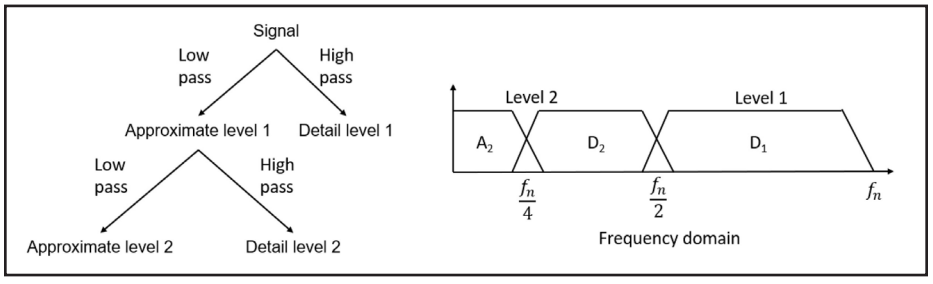

Figure 8 Discrete wavelet transform (a) multiresolution analysis flow chart (b) frequency coverage of coefficients.

Table 3 Synthetic profile harmonic content

Amplitude in µm	Order	Location
2	1	Full trace
1	7	Full trace
1	9	Full trace
0.5	30	Full trace
0.5	50	40 to 50 mm length of roll

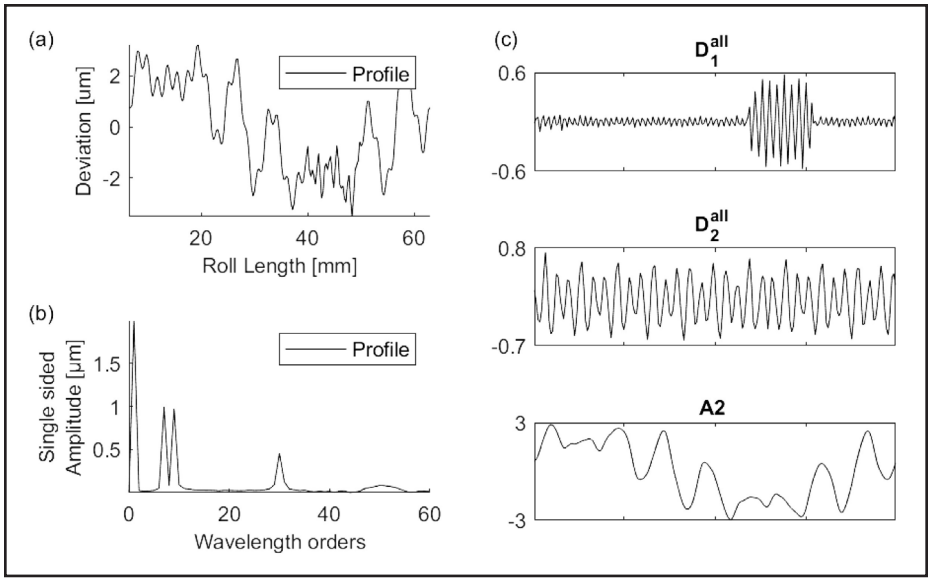

Figure 9 Synthetic profile (a) trace (b) DFT single sided spectrum results limited to 60 orders (c) DWT levels of detail.

the two inversion methods with and without fitting of r_b is discussed based on Figure 7. $\Delta F(S)$ is calculated with the Euclidean norm of the distance between $F(S)$ without and with fitting of r_b. $\Delta F(S)$ is shown at the coordinates of the form element S determined with fitting of r_b. Whenever nominal and actual r_b are particularly far away from each other, the gear flanks are depicted in red as a function of the radius as illustrated on tooth 2 and tooth 4. This effect is particularly significant close to the base and addendum circle.

Tooth 4 will be investigated in Section 4.3 in detail. On tooth 4, the conventional from deviations of profile, helix (VDI/VDE 2021-1:2018(E), Ref. 2) and pitch (VDI/VDE 2613:2003, Ref. 3) taken from the measuring protocol of the CMM are:

$f_{H\alpha}{}^{le} = -9.256\,\mu m$ and $f_{H\alpha}{}^{ri} = -12.763\,\mu m$ at $L_{AE} = (153.530–196.000)\,mm$

$f_{H\beta}{}^{le} = -1.194\,\mu m$ and $f_{H\beta}{}^{ri} = -3.468\,\mu m$ at $b = 110.000\,mm$

$F_p{}^{le} = 6.384\,\mu m$ and $F_p{}^{ri} = 15.578\,\mu m$ at $r = 111.277\,mm$

Analysis of Harmonic Content

Harmonic Evaluation Methodology Background

The discrete Fourier transform (DFT) splits a signal into sine waves and is used in numerous applications to analyze the frequency content of a signal. It is calculated using the fast Fourier transform (FFT) — an optimized implementation of the DFT (Ref. 15). The Fourier transform has only frequency resolution and no position resolution, computing only if a frequency occurs across the whole signal but not where it occurs.

The discrete wavelet transform (DWT) splits a signal using wavelets (Ref. 16). Many different wavelets exist and can be tuned for specific applications (Refs. 17–20). Discrete wavelets are not continuous and are scaled and translated to discern information about both frequency and position. A common strategy with a wavelet transform is multiresolution analysis, where the signal is split into sub-signals which represent different frequency ranges of the original. This works as a filter bank where the signal is high and low passed, using the wavelet as the filter, splitting

the signal into detail and approximate sub-signals relating to high and low frequency content respectively, as seen in Figure 8a (Ref. 21). At the next level the approximate signal is split again covering successively narrower frequency bands (Fig. 8b). This has the effect of giving greater resolution in time for higher frequency content which allows us to know information about the position of frequency as well as the order.

The signal can be reconstructed at any level of detail by combining the lowest level approximate sub-signal and the related detail sub-signals. This is useful because machining or surface finish characteristics can be limited to a frequency range which when separated are easier to understand. ISO 16610-29:2020 performs a multiresolution analysis using spline wavelets and has examples for a milled surface and ceramic surface (Ref. 22).

2D Trace Analysis

A synthetic profile has been constructed with the harmonic content in Table 3 to demonstrate the two transforms. The 50th order harmonic occurs over a section of profile to provide a simple representation of a damaged region, or a region affected by temporary vibration of a machine tool. The synthetic trace and analysis by DFT and DWT are shown in. The DWT was used to perform a two-level multiresolution analysis using Daubechies wavelet 6 (db6).

Considering the DFT single sided frequency spectrum (Fig. 9b), the harmonic amplitudes have been correctly calculated for the first four harmonics but the 50th order harmonic amplitude cannot be discerned and is spread around several orders. However, the DWT has correctly identified the existence of the 'damage' in the detail level 1. It is not possible from Figure 9c to identify specific harmonic frequencies but the effect of harmonic content from a range of frequencies can be seen in each subplot with orders 1, 7, and 9 in A2, order 30 split between D2 and D1, and finally order 50 in D1.

Tooth four measured mid profile inverted with base radius fitting has been analyzed in Figure 10. The deviations are from the involute form element in the transverse plane. A 1st order sine wave is obvious in the DFT plot (Fig. 8b) with an amplitude of almost 0.7 microns, with the next highest at the 5th order with an amplitude of 0.25 microns. Otherwise, there is no obvious other harmonic peaks, a common problem with high quality gears where the deviations, and thus harmonic amplitudes, are very small.

The DWT (Fig. 10c) highlights a waviness profile in D2 and D1 with a range of 0.6 microns. This is where the DWT and multiresolution analysis can be useful to monitor machine tool performance or surface finish performance. For example, cutting errors due to machine tool vibrations may not be in the same coordinate axes and will not directly relate to a harmonic in the DFT plot, or may not exist for the full cutting time and would then be spread around the frequency plot. The DWT levels of detail show the effect of vibrations without having to know the frequency.

Another example of this is in Figure 11, which is the same profile but evaluated without fitting the actual base radius and exaggerated profile slope. Without first removing the slope or windowing the signal the DFT plot (Fig. 11a) has many frequencies spread across the spectrum obscuring any useful frequency information. However,

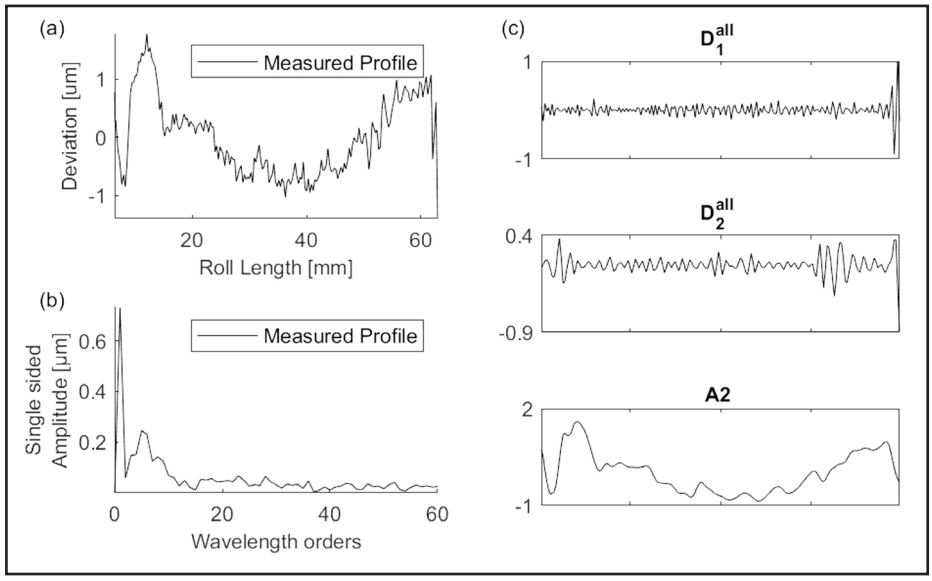

Figure 10 Measured profile fitted with rb (a) trace (b) DFT single sided spectrum results limited to 60 orders (c) DWT levels of detail.

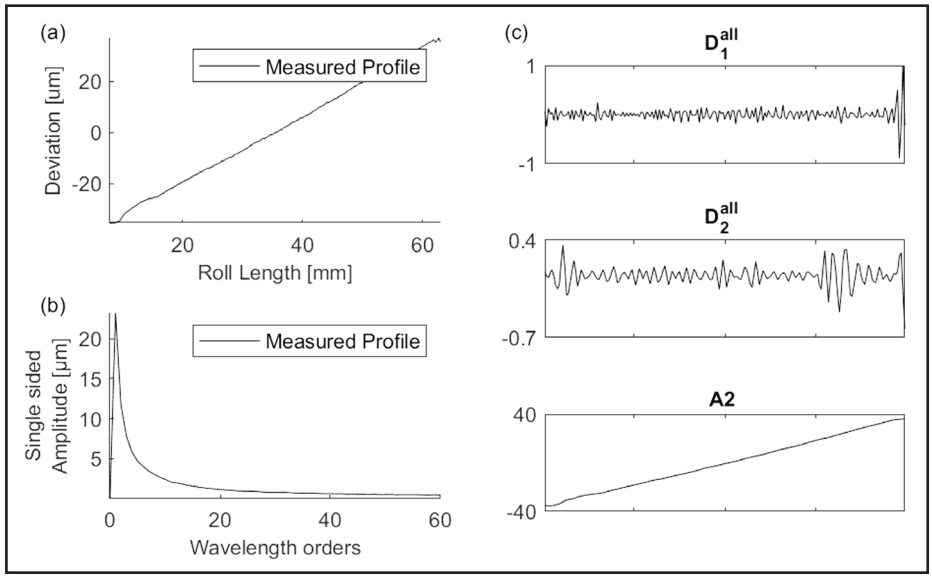

Figure 11 Measured profile fitted without rb (a) trace (b) DFT single sided spectrum results limited to 60 orders (c) DWT levels of detail.

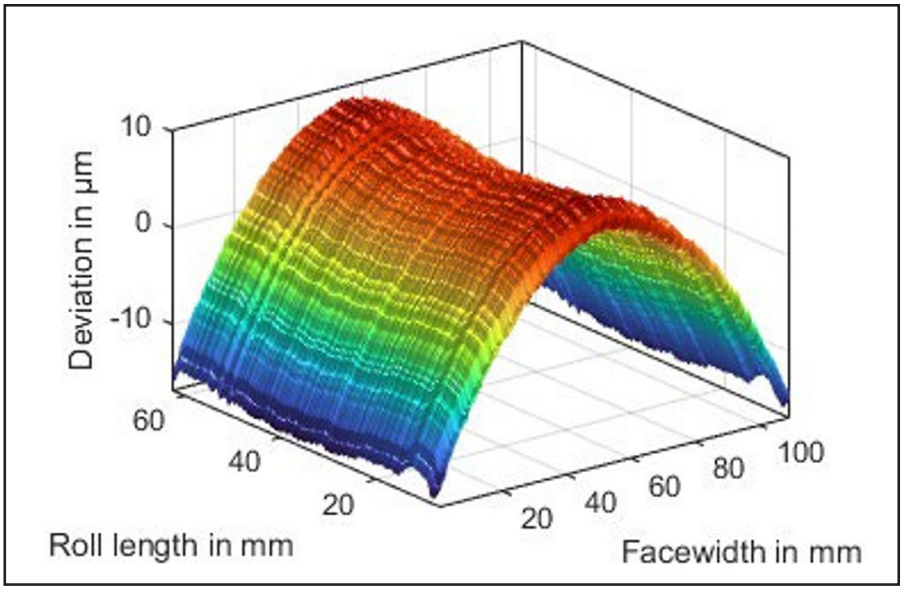

Figure 12 Tooth 4 pseudo-measured surface.

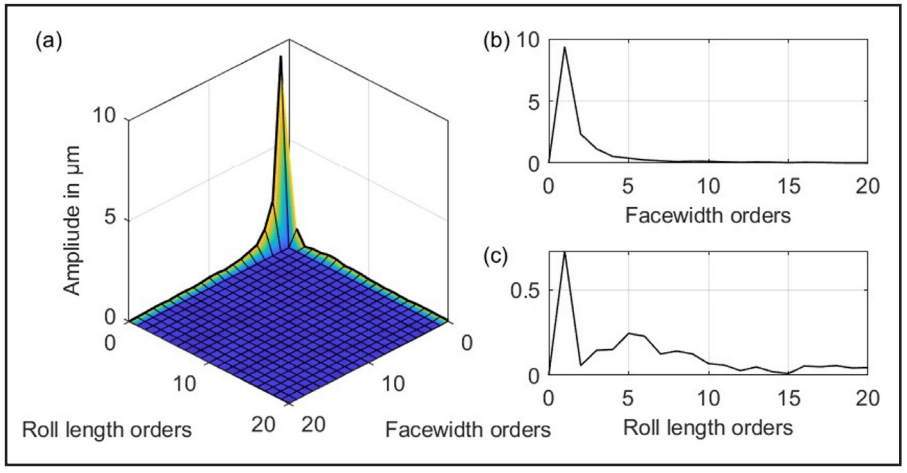

Figure 13 Surface DFT amplitudes limited to 20 orders (a) isometric view (b) face width order slice (c) roll length order slice.

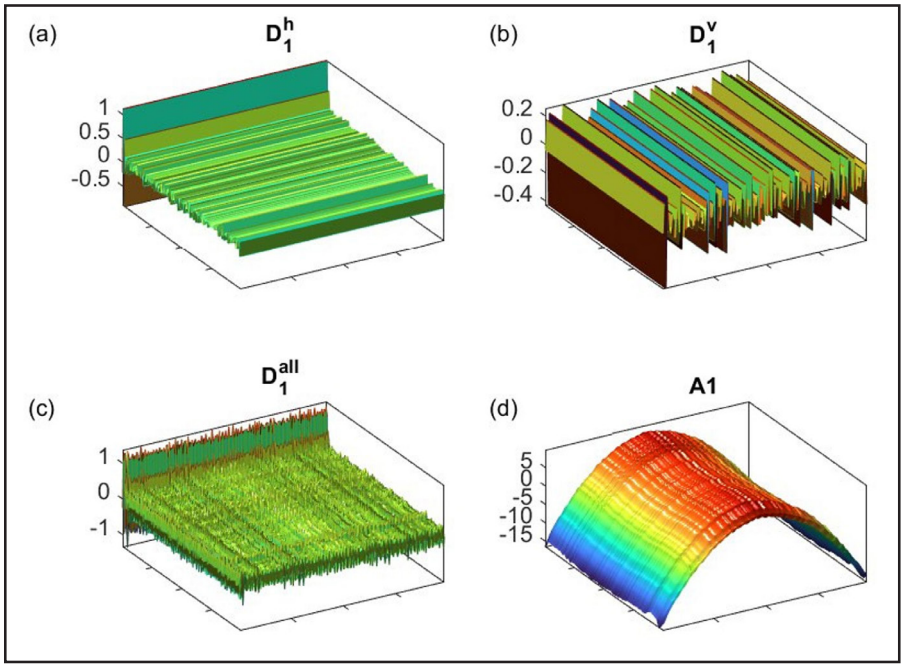

Figure 14 Surface DWT (a) horizontal, (b) vertical, (c) combined detail surfaces and (c) approximate surface.

the DWT filters this out at the approximate level leaving the higher frequency information visible in the detail levels.

3D Surface Analysis

Extending the 2D methods to 3D is simple to compute but complex to understand. A pseudo-measured surface has been created for analysis by layering tooth four mid profile and helix (fitted with r_b deviations) into a grid, giving the surface in Figure 12 (L, b, and d refer to roll length, face width, and deviation from involute respectively).

Discrete Fourier Transform

The 2D DFT amplitudes are shown in Figure 13 in isometric view and with slices of the roll length and face width harmonics. Two perpendicular lines of content can be seen which relate to the face width and roll length orders. If there was any harmonic content at an angle, such as produced with generator grinding, a corresponding angled line would be visible.

In this case the frequencies have been dominated by the DFT trying to describe a 0.5 order harmonic — the helix crowning in Figure 12. This will be a common problem for gears which will typically have some sort of microgeometry correction as in the example discussed here. A solution would be to window the surface before transforming or to fit the microgeometry and remove this before analyzing harmonics.

Discrete Wavelet Transform

Extending the DWT to 3D adds even more complexity as at each level of detail a surface is split into one approximate and three detail sub-surfaces: horizontal, vertical, and diagonal. Figure 14 shows a one level DWT using Daubechies wavelet 6 (db6). The following should be noted:

- The approximate surface has separated out the crowning and some low frequency profile effects
- Horizontal detail relates to profile harmonics and a has a similar shape to the combined D1 and D2 of Figure 9c
- Vertical detail relates to helix harmonics
- The diagonal detail deviations were negligible at 10^{-15} µm and are not shown

- D^{all} is a combination of the horizontal, vertical, and diagonal details

Discussion and future work

The 3D-evaluation approach presented here is suitable to determine individual manufacturing errors on each gear tooth. An error separation method has been applied that includes the 3D measuring strategy on CMMs and the holistic point cloud inversion by separating running, geometry, and pose parameters. In the end one set of geometry parameters per gear flank is determined in a common reference system. In addition, two possible methods of evaluating measured point clouds were presented. The base radius, one of three geometry parameters in the 3D-gear surface model, has been either fitted during the inversion or not. Observed differences are listed in the following. Merits and drawbacks are denoted by (+) and (–).

Comparing inversion methods

+ Inversion with fitting of r_b enables the determination of the actual geometry parameters per gear flank: $r_{b,act}$ φ_b and β_b.
– Inversion without fitting of r_b results in $r_{b,nom}$ that has an effect on the other actual geometry parameters φ_b and β_b. Compared to the alternative approach, it has been observed that the fitted φ_b and β_b compensate for the incorrect radius, so that other actual geometry parameters are obtained.
– Inversion without fitting of r_b results in residuals with an artificial slope error. When analyzing the harmonics, this error leads to polluted FFT spectra. The DWT filters out the slope at the approximated level of detail are not affected.

Comparing harmonic methods

+ FFT shows specific harmonic frequency and amplitude
– FFT cannot discern content that exists for only a portion of the measurement
– FFT spectrum gets polluted by slope errors or other common microgeometry corrections, especially if the base radius has not been fitted in the previous inversion of point clouds
± DWT does not show specific frequencies but can show the effect of a frequency band
+ DWT can discern the location of content that exist for only a portion of the measurement
+ DWT filters can filter out slope errors and common microgeometry corrections in the lowest approximate level

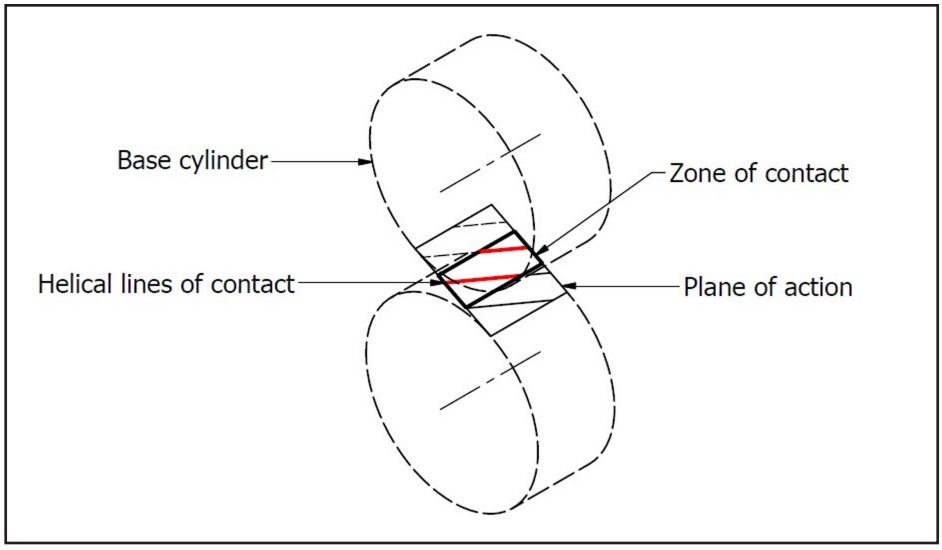

Figure 15 Lines of contact.

Analyzing a surface compared to a 2D line trace provides additional information about the whole flank and allows for better understanding of errors from machine tools, predicts potential vibration issues or detects damage that is not captured within a single profile and helix trace.

This is useful but analyzing an individual gear flank surface geometry to understand how these errors relate to the gear's performance is difficult as best and misleading at worst. This is particularly the case for helical gears with angled lines of contact (Figure 15) over the tooth surface. Pinion and wheel gear pair surfaces combine, at different points in time different number of teeth are in contact, gears run eccentrically in bearings and then when load is applied, gear teeth and shafts deflect. All of these obfuscate the effect of measured harmonics on the functional performance of the gear.

The obvious next step is to use the measured data in a tooth contact analysis (TCA) model. These models usually assume nominal macro and micro geometry or at best consider ranges to profile and helix deviation slope limits and micro geometry corrections to predict gear performance. However, we can import the actual measured 3D surface deviations into TCA models to predict gear performance in terms of transmission error, bending and contact stress, scuffing risk and friction losses (Ref. 23). We can then use these results to determine fitness for purpose directly or develop tolerances based on modeled performance if the TCA model has been verified. This may be of real benefit for high value gears used in, for example, wind turbine gearboxes.

Harmonic analysis characterization can also be useful as a method for robustly and efficiently transferring the measured 3D surface deviations to TCA models and digital twin models. By using the data from these transforms, the surface can be defined to an appropriate resolution by controlling how many harmonics to include in the deviation surface characterization. The resolution may be different based on the desired performance to modelled. For example, if noise was more important for a certain application, fewer harmonics are required to characterize this compared to the requirements of contact stress or scuffing risk simulations. The DFT and DWT are reversable and can be used by the TCA program to reconstruct the surface to the resolution defined by the metrologist, blurring the lines between design and metrology.

Acknowledgements

The project 19ENG07 Met4Wind has received funding from the EMPIR program co-financed by the Participating States and from the European Union's

Horizon 2020 research and innovation program.

References

1. ISO 1328, 2013, "Cylindrical gears – ISO system of flank tolerance classification – Part 1: Definitions and allowable values of deviations relevant to flanks of gear teeth," ISO 1328-1:2013(E).
2. VDI/VDE, 2018, "Measurement and testing of gears – Evaluation of profile and helix measurements on cylindrical gears with involute profile," VDI/VDE 2021-1:2018(E).
3. VDE/VDI, 2003, "Pitch and runout testing on gearings: Cylindrical gears, worm wheels, bevel gears," VDI/VDE 2613:2003.
4. Frazer, R. C. et al., 2003, "An international comparison of involute gear profile and helix measurement," *Metrologia*, Vol. 41, No. 1, pp. 12–16.
5. Härtig, F. and Kniel, K., 2014, "First International Involute Gear Comparison," *Gear Technology*, August 2014, pp. 80–84.
6. Peng, Y. et al., 2018, "Areal Evaluation of Involute Gear Flanks with 3D Surface Data," AGMA Fall Technical Meeting in Columbus, American Gear Manufacturers Association (AGMA), Columbus, Ohio, pp. 42–51.
7. Goch, G. et al., 2017, "Future gear metrology based on areal measurements and improved holistic evaluations," *CIRP Annals - Manufacturing Technology*, Vol. 66, No. 1, pp. 469–474.
8. Müller, H. 2016, "Noise generation in gearings: see no evil, hear no evil, speak no evil" [White paper]. Klingelnberg Gmbh. *https://www.klingelnberg.com*
9. Wagaj, P., and Beerck, D., 2019, "Gear Noise Analysis: design and manufacturing challenges drive new solutions for noise reduction," *Gear Technology*, July 2019, pp. 42–49.
10. Dale, A. K., 1987, "Gear Noise and the Sideband Phenomenon", *Gear Technology*, January/February 1987, pp. 26–33.
11. Gravel, G. 2012, "Analysis of ripple on noisy gears," AGMA Fall Technical Meeting 2012.
12. Zargarbashi, S., and Angeles, J., 2014, "Identification of error sources in a five-axis machine tool using FFT analysis," *The International Journal of Advanced Manufacturing Technology*, 76(5–8), pp. 1353–1363.
13. Härtig, F. and Stein, M., 2019, "3D involute gear evaluation – Part I: Workpiece coordinates," *Measurement*, 134, pp. 569–573.
14. Sourlier, D. and Bucher, A., 1992, "Exact bestfit algorithm applicable to sculptured surfaces or to any non-regular surfaces in parametric form," *tm - Technisches Messen*, 59(7–8), pp. 293–302.
15. Cooley, J., and Tukey, J., 1965, "An algorithm for the machine calculation of complex Fourier series," *Mathematics of Computation*, 19(90), pp. 297–297.
16. Burrus, C., R. Gopinath, Haitao Guo, J. E. Odegard and I. Selesnick. "Introduction to Wavelets and Wavelet Transforms: A Primer." (1997).
17. Haar, A., 1911, "Zur Theorie der orthogonalen Funktionensysteme," Mathematische Annalen, 71(1), pp. 38–53.
18. Wirsing, K., 2014, "Application of Wavelets to Filtering and Analysis of Self-Similar Signals," Masters, Virginia Polytechnic Institute and State University.
19. Daubechies, I., 1988, "Orthonormal bases of compactly supported wavelets," Communications on Pure and Applied Mathematics, 41(7), pp. 909–996.
20. Merry, R. "Wavelet theory and applications: a literature study." (2005).
21. Valens, C. "A Really Friendly Guide to Wavelets." (1999).
22. ISO, 2020, "Geometrical product specifications (GPS). Filtration. Linear profile filters: Wavelets," ISO 16610-29:2020.
23. 2021, *Gear Production Suite*, Dontyne Systems.

Anita Przyklenk obtained a BSc, MSc and Ph.D. in Physics from TU Braunschweig, Germany. Since 2018, she is a postdoctoral research fellow at Physikalisch-Technische Bundesanstalt (PTB) in the working group for gear and thread metrology. Her research topic is three-dimensional and holistic gear and screw thread evaluation methodology. She is the Secretary of the European Metrology Network for Advanced Manufacturing by the European Association of National Metrology Institutes (EURAMET).

Tom Reavie joined Newcastle University's Design Unit in 2017 after completing his master's degree in mechanical engineering. His work involves design of mechanical power transmissions with a focus on gear design and analysis. Tom is a member of the UK's National Gear Metrology Laboratory (NGML) and he is completing a Ph.D. alongside his research in gear metrology.

Martin Stein has studied mathematics and physics at Leibniz University Hanover, Germany, and finished his Ph.D. in 2012. He's been heading the working group for gear and thread metrology at Physikalisch-Technische Bundesanstalt (PTB) since 2014. One of that group's main research areas is metrology for large gears as used in wind energy systems. Martin Stein is an active member in national standardization bodies for gear metrology of the VDI/VDE and DIN. He is a lecturer at TU Braunschweig for the MSc course on Metrology and Measurement Technology.

Rob Frazer received a BSc in Mechanical Engineering and Ph.D. from Newcastle University. He is a senior engineer with the Design Unit at Newcastle University and spent the last 35 years working with gears and gearboxes. Rob leads gear measurement research at the UK's National Gear Metrology Laboratory (NGML), is chair of British Standard Institute (BSI) gear committee, MCE-5 and a member of the ISO gear accuracy working group (ISO TC60 WG2). He provides technical support to the British Gear Association's (BGA) research committee, helps deliver its training programmes and teaches on Newcastle University's MSc and MEng Mechanical Power Transmissions Module.